2021 IEEE International Conference on Robotics and Automation (ICRA 2021)
May 31 - June 4, 2021, Xi'an, China

# Toward Autonomous Driving by Musculoskeletal Humanoids: A Study of Developed Hardware and Learning-Based Software

Kento Kawaharazuka[1], Kei Tsuzuki[1], Yuya Koga[1], Yusuke Omura[1], Tasuku Makabe[1], Koki Shinjo[1]
Moritaka Onitsuka[1], Yuya Nagamatsu[1], Yuki Asano[1], Kei Okada[1], Koji Kawasaki[2], and Masayuki Inaba[1]

***Abstract*— This paper summarizes an autonomous driving project by musculoskeletal humanoids. The musculoskeletal humanoid, which mimics the human body in detail, has redundant sensors and a flexible body structure. These characteristics are suitable for motions with complex environmental contact, and the robot is expected to sit down on the car seat, step on the acceleration and brake pedals, and operate the steering wheel by both arms. We reconsider the developed hardware and software of the musculoskeletal humanoid Musashi in the context of autonomous driving. The respective components of autonomous driving are conducted using the benefits of the hardware and software. Finally, Musashi succeeded in the pedal and steering wheel operations with recognition.**

## I. INTRODUCTION

As a means of safe and comfortable transportation, various researches in autonomous driving are in progress [1], [2]. Some companies have achieved a certain level of autonomous driving, e.g. headway vehicle following and autonomous parking. These cars are equipped with powerful cameras, LiDARs, GPS, and processors for accurate and safe control.

On the other hand, starting with the autonomous driving task at DARPA Robotics Challenge (DRC) [3], there are researches on autonomous driving by humanoid robots [4], [5]. Humanoid robots are equipped with various sensors for visual, acoustic, and force information. By using these sensors, the robot can get into the car and drive instead of humans. Also, unlike ordinary autonomous driving, the humanoid robot is expected to do other various tasks, e.g. carrying heavy baggage, assisting the old, doing housework, and aiding with disaster response. However, because the humanoid robot lacks the flexibility of the body and deviates from the human body proportion, in DRC, a steering wheel was operated by one arm and a special jig was required to sit down on the seat.

Although various kinds of humanoid robots exist, one that imitates the human actuation system is the musculoskeletal humanoid [6]–[9]. The musculoskeletal humanoid is actuated not by motors arranged at each axis but by pneumatic actuators or muscle actuators with motors that imitate human muscles. The body is flexible compared with the ordinary axis-driven humanoid due to the muscle elasticity and under-actuation, and so it is suitable for motions with complex environmental contact. Therefore, the musculoskeletal humanoid can sit down on the car seat easily without a special jig and operate the steering wheel flexibly by both arms. Also, this robot can be used as a more realistic crash test dummy [10] because of the human-like body structure and actuation.

Fig. 1. Autonomous driving by musculoskeletal humanoids

In this study, we introduce our project of autonomous driving by musculoskeletal humanoids (Fig. 1). Especially, we describe the characteristics of the hardware and learning-based software to move the flexible body. We reconsider the developed hardware [9], [11]–[13] and software [14]–[16] in the context of autonomous driving. Also, we develop the respective components of autonomous driving and conduct experiments integrating them using the hardware and software characteristics.

This paper is organized as follows. In Section II, we will explain the characteristics of the developed hardware and their applications to autonomous driving. In Section III, we will explain the overview of the learning-based software and their application to autonomous driving. In Section IV, we will integrate the hardware and software, and conduct experiments of the pedal and handle operations with recognition. In Section V, we will discuss the issues of each experiment and future directions, and finally conclude this project in Section VI.

## II. HARDWARE OF THE MUSCULOSKELETAL HUMANOID

### A. Design Process

The important points for a robot to drive a car made for humans are considered to be (1) body proportion, (2) body flexibility, and (3) redundant sensors and learning system using them. In this paper, (1) we first determine the arrangement of joints and the length of each bone to fit the proportion and joint structure of humans, and attach muscle modules to the bones. In addition, (2) a nonlinear elastic unit is attached to the end of each muscle, and the robot can fit into the complex environment with the unit and the original flexibility of muscle wire. Finally, (3) we design a structure including not only the muscle module

[1] The authors are with the Department of Mechano-Informatics, Graduate School of Information Science and Technology, The University of Tokyo, 7-3-1 Hongo, Bunkyo-ku, Tokyo, 113-8656, Japan. kawaharazuka@jsk.t.u-tokyo.ac.jp
[2] The author is associated with TOYOTA MOTOR CORPORATION.

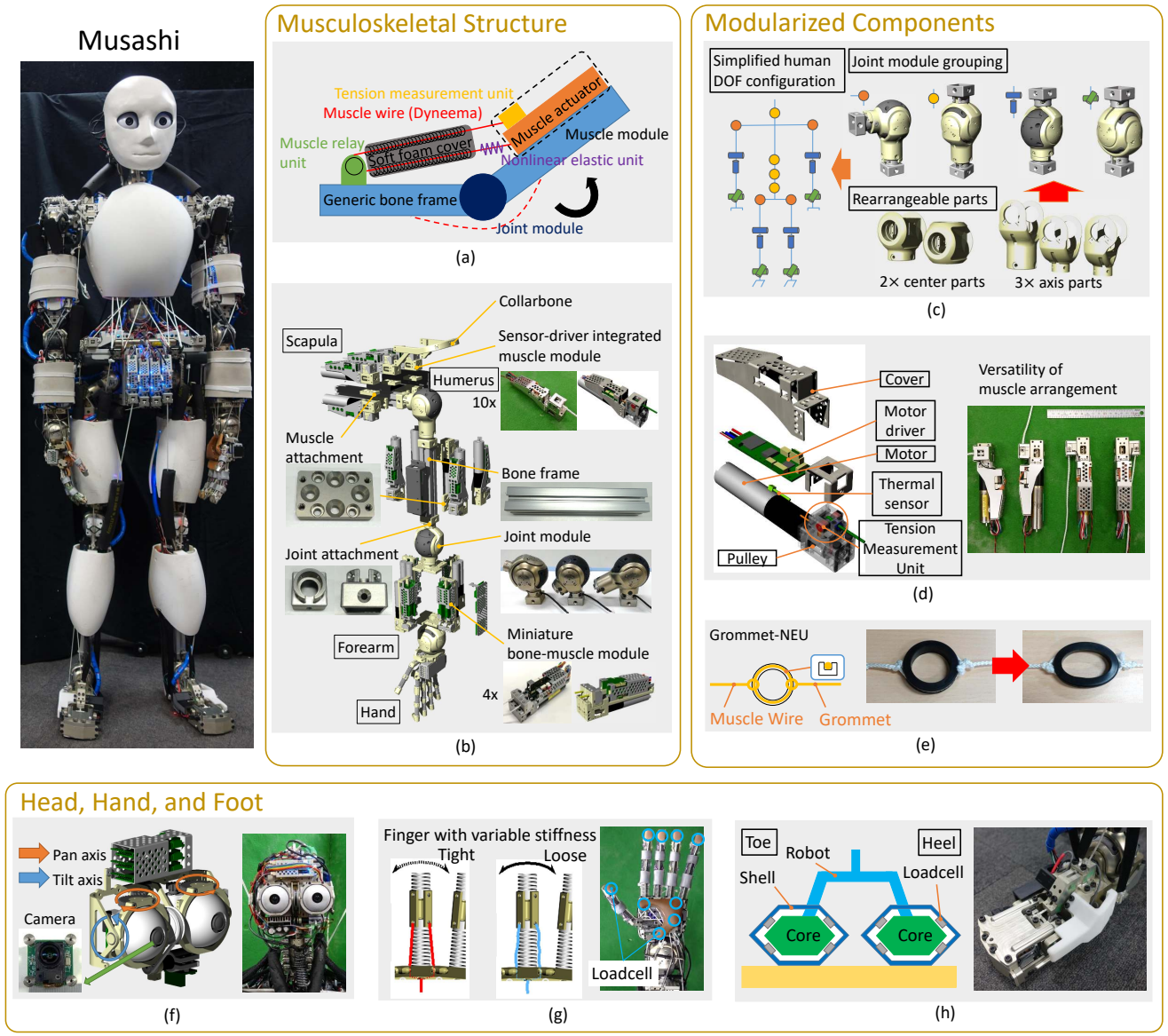


Fig. 2. The overview of the developed musculoskeletal humanoid Musashi. (a) shows the basic musculoskeletal structure. (b) shows the modularized structure of the left arm of Musashi combining various modules, (c) shows the rearrangeable concept of joint modules. (d) shows the detailed structure of muscle module (left figure) and the versatility of muscle arrangement (right figure). (e) shows the nonlinear elastic unit. (f) shows the movable eye unit. (g) shows the flexible musculoskeletal hand with machined springs. (h) shows the foot with six-axis core-shell structural force sensors.

that can measure muscle length, muscle tension, and muscle temperature, but also a flexible hand with contact sensors, movable eyes with high resolution cameras, and loot with 6-axis force sensors that can measure force around their entire surface, as redundant sensors. In the next section, we will describe in detail the design of muscle modules and nonlinear elastic units that form (2), and joint modules, eyes, hands and foot that form (3).

### *B. Hardware Details*

We show the hardware overview of the developed musculoskeletal humanoid Musashi [9] in Fig. 2. Currently, Musashi has 74 muscles and 39 joints excluding the hand.

(a) shows the basic musculoskeletal structure of Musashi. The joint module connects the generic bone frames, and muscle modules are attached to the frame. The abrasion-resistant synthetic fiber Dyneema comes out as a muscle from the tension measurement unit of the muscle module and is folded back by the muscle relay unit. The nonlinear elastic unit is attached to the end of the muscle, and a soft foam and spring covers the muscle. Muscles are antagonistically arranged around the joint. We describe muscles mainly conducting the current task as agonist muscles and the others as antagonist muscles.

(b) is the structure of the left arm of Musashi constructed by the modules of (c) – (e) explained subsequently. The body structure is easily constructed by the modules, muscle attachments connecting bones and muscles, and joint attachments connecting bones and joints.

(c) shows the detailed structure of the joint module. We can express all the basic human joints by rearranging two center parts and three axis parts. Potentiometer, IMU,

and a circuit integrating sensor data are packaged in the joint module. We can change the body structure easily by transforming this joint module.

(d) is the detailed structure of the muscle module. We use two kinds of muscle modules depending on the body part. One of them is a sensor-driver integrated muscle module [17], which can drastically improve reliability and maintainability by packaging a motor, motor driver, thermal sensor, tension measurement unit, etc. into one module. The muscle is actuated by winding a muscle wire with a pulley. The other is a miniature bone-muscle module [18]. Although the basic concept is the same with [17], the module is used not only as a muscle but also as a bone frame, and dissipates heat to metal by packaging two smaller actuators into one module and filling the space between the two actuators by metal. We can get muscle tension, length, and temperature as sensor data. Also, as shown in the right figure of (d), we can realize various muscle routes by rearranging the tension measurement unit.

(e) shows the nonlinear elastic unit (NEU). The previous NEUs are constructed by metal and springs, and the structure is not appropriate for environmental contact. Therefore, we realize the nonlinear elasticity using the compression of rubber, by covering the grommet rubber with Dyneema. Because the NEU is constructed with only rubber and Dyneema, the structure itself is flexible, and it is suitable for environmental contact.

(f) is the head of Musashi with the movable eye unit [11]. The unit includes three joints: a pan joint in each eye and a tilt joint. We use DFK-AFUJ003 (ImagingSource, Inc.) as the eyes, and we can change the image resolution, focus, exposure, etc. Although we considered using Lidars/Radars, we decided consistently to mimic the structure of human beings in detail.

(g) is the hand of Musashi with machined springs [12]. The hand does not break even if hit by a hammer because of the high flexibility. Muscles are antagonistically arranged at proximal phalanges of each finger, and the finger stiffness can be changed by pulling the muscles and compressing the springs. Nine loadcells are arranged at each fingertip and the palm of each hand, and contact force can be measured from them.

(h) is the foot of Musashi with six-axis core-shell force sensors [13]. The core-shell structure is arranged at the toe and heel, and multiple loadcells are arranged between the core and shell. This structure can measure all the force applied to the entire shell surface, and so the force to the instep of the foot can be measured.

### C. Application of the Hardware to Autonomous Driving

We explain the use of the developed nonlinear elastic unit, head, hand, and foot of Musashi in terms of autonomous driving, in Fig. 3 (presented in multimedia material).

By using nonlinear elastic units, the robot can not only make the body flexible but can also change the stiffness freely. As shown in (a), the flexible body structure makes it possible to operate a steering wheel with both arms, which

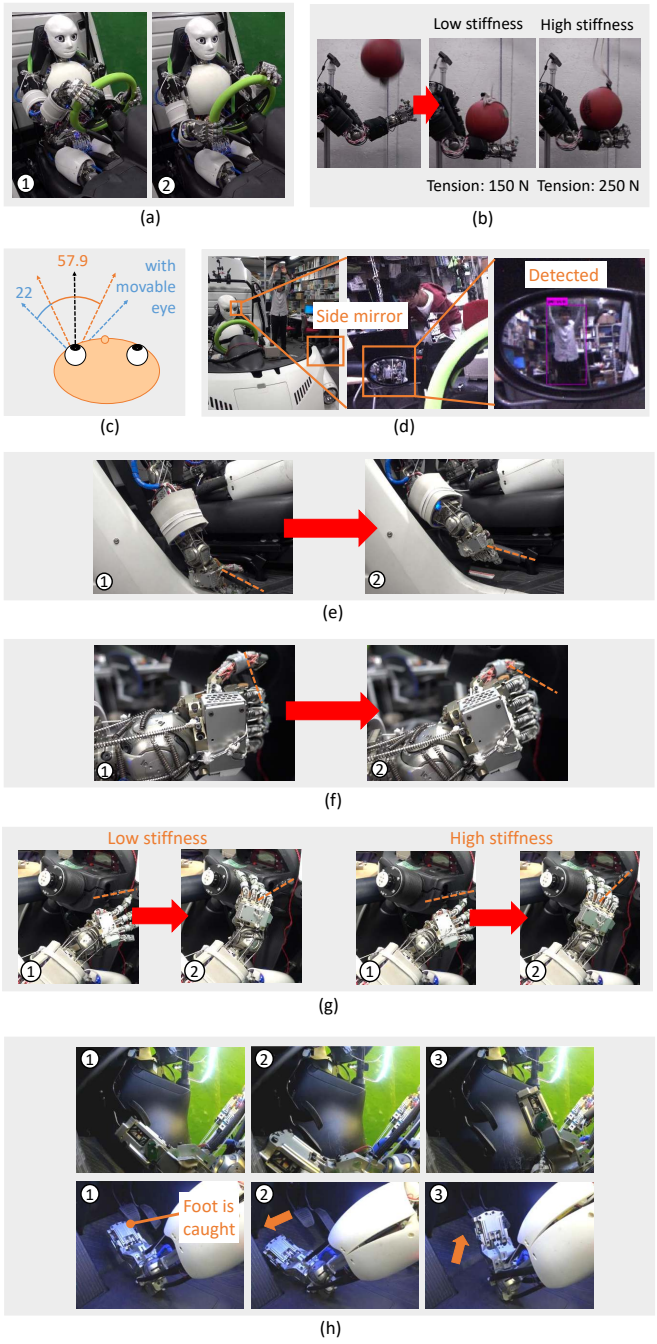


Fig. 3. The realization of respective components of autonomous driving using the characteristics of the developed hardware. (a) shows a steering wheel operation with both arms. (b) shows a variable stiffness control using the nonlinear elastic units. (c) shows the field of view of the movable eye unit. (d) shows the human detection experiment in the side mirror using the high resolution camera. (e) shows an experiment pulling a handbrake. (f) shows an experiment rotating a key. (g) shows an experiment operating a blinker lever by changing the stiffness of fingers. (h) shows a recovering experiment from slipping during brake pedal operation using the developed foot.

could not be seen in DRC. Also, as shown in (b), the robot can change impact response by changing the body stiffness. When dropping a 5 kg ball to the robot from 1 m height, the maximum muscle tension is 150 N with low stiffness, and 250 N with high stiffness. This resembles the increase

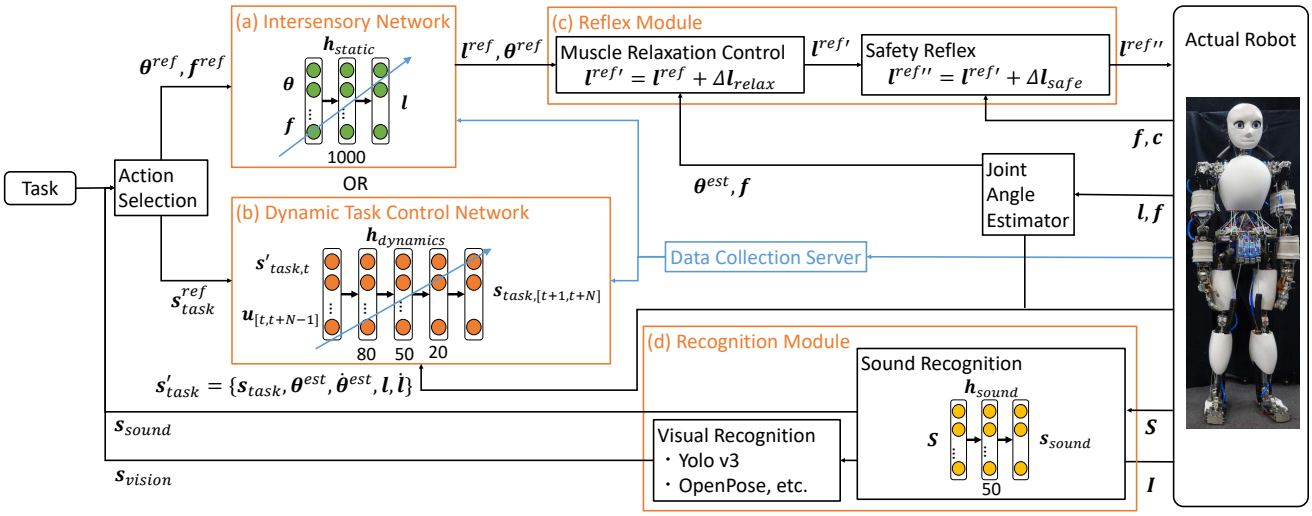


Fig. 4. The overview of the developed software with four modules: intersensory network module (static module), dynamic task control network module (dynamic module), reflex module, and recognition module.

of human arm stiffness during a car crash, and the use of Musashi as a crash test dummy is anticipated.

By using the head with the movable eye unit, the robot can recognize objects with a wide field of view as shown in (c). Also, the robot can recognize a human in a side mirror using the high resolution camera, as shown in (d).

By using the flexible hand with machined springs, the robot can adapt the grasp shape to various situations inside the car, such as pulling a handbrake (e) and rotating a key (f). Also, by using the variable stiffness mechanism of fingers, as shown in (g), the robot can operate a blinker lever correctly with high stiffness.

By using the foot which can measure the force applied to its entire surface, the robot can recover the foot position by sensing the force to its instep when slipping during a brake pedal operation, as shown in (h).

## III. Software of the Musculoskeletal Humanoid

### A. Design Process

In order to handle the flexible body and redundant sensors, we consider that (1) a learning-based motion generation, (2) a learning-based recognition, and (3) a fast reflex control are necessary. (1) can be divided into two types of motion generators, for static behavior and dynamic behavior. In the former, the dimension of state space is relatively small and online learning is effective. In the latter, the dimension is relatively large and only offline learning can be used currently. In addition, we also develop (2) learning-based recognition methods using eyes and ear sensors, because visual and sound recognition is significant in performing the driving task. Since it is difficult to operate learning-based controls at high frequency, a safety mechanism should be implemented in a lower layer as (3) reflex control. In this study, we use a simple conditional branching based on the recognition results for motion planning.

### B. Software Details

We show the overview of the learning-based software system in Fig. 4. We describe the current muscle length as $\boldsymbol{l}$, the current muscle tension as $\boldsymbol{f}$, the current joint angle as $\boldsymbol{\theta}$, the current muscle temperature as $\boldsymbol{c}$, the muscle Jacobian as $G$, the current image as $\boldsymbol{I}$, the current sound as $\boldsymbol{S}$, the task state as $\boldsymbol{s}_{task}$, the current state obtained from vision as $\boldsymbol{s}_{vision}$, and the current state obtained from sound as $\boldsymbol{s}_{sound}$. Also, $\{\boldsymbol{l}, \boldsymbol{\theta}, \boldsymbol{f}, \boldsymbol{s}_{task}\}^{ref}$ is the control command of each state, and $\boldsymbol{\theta}^{est}$ is the estimated joint angle.

The basic components of this system are (a) intersensory network module (static module), (b) dynamic task control network module (dynamic module), (c) reflex module, and (d) recognition module.

The static module (a) acquires the function $\boldsymbol{h}_{static}$ below [14].

$$\boldsymbol{l} = \boldsymbol{h}_{static}(\boldsymbol{\theta}, \boldsymbol{f}) \tag{1}$$

This represents the static relationship among $\boldsymbol{\theta}$, $\boldsymbol{l}$, and $\boldsymbol{f}$. When $\boldsymbol{\theta}^{ref}$ and $\boldsymbol{f}^{ref}$ are given depending on the task, by inputting them into Eq. 1, $\boldsymbol{l}^{ref}$ to send to the robot is calculated. This function is expressed by a neural network, and is initialized by man-made data. Then, we update the network online by using the actual robot sensor information $(\boldsymbol{\theta}, \boldsymbol{f}, \boldsymbol{l})$. At every movement, the network is updated, and the robot becomes able to realize $\boldsymbol{\theta}^{ref}$, $\boldsymbol{f}^{ref}$ accurately. In this study, $\boldsymbol{\theta}$ can be obtained from the joint module, but the ordinary musculoskeletal humanoid does not have joint angle sensors due to complex joints such as the ball or scapula joints. In that case, $\boldsymbol{\theta}$ must be obtained from a motion capture or vision sensor. Also, by using this network $\boldsymbol{h}_{static}$, not only control but also estimation of joint angles $\boldsymbol{\theta}^{est}$ are enabled by using Extended Kalman Filter (EKF) and the change in muscle length and tension.

The dynamic module (b) acquires the function $\boldsymbol{h}_{dynamic}$ below [15],

$$\boldsymbol{s}_{task,[t+1,t+N]} = \boldsymbol{h}_{dynamics}(\boldsymbol{s}'_{task,t}, \boldsymbol{u}_{[t,t+N-1]}) \tag{2}$$

where $\{\boldsymbol{s}_{task}, \boldsymbol{u}\}_{[t_1,t_2]}$ is a vector vertically arranging $\{\boldsymbol{s}_{task}, \boldsymbol{u}\}$ from $t_1$ to $t_2$ time steps, $\boldsymbol{s}'_{task,t}$ is the initial task state ($\{\boldsymbol{s}_{task}, \boldsymbol{\theta}^{est}, \dot{\boldsymbol{\theta}}^{est}, \boldsymbol{l}, \dot{\boldsymbol{l}}\}$ in this study), $\boldsymbol{u}$ is the control command ($\boldsymbol{\theta}^{ref}$ or $\boldsymbol{l}^{ref}$ in this study), and $N$ is the number of time steps to expand this state equation. This function is equivalent to a network representing a dynamic transition of the task state by a control command sequence. This network can be trained by gathering data of observed task state transition when sending random control commands. When realizing a certain task state $\boldsymbol{s}^{ref}_{task}$, we execute the equations below after setting the initial $\boldsymbol{u}$,

$$\boldsymbol{s}^{pred}_{task,seq} = \boldsymbol{h}_{dynamic}(\boldsymbol{s}'_{task,t}, \boldsymbol{u}^{init}_{seq}) \tag{3}$$

$$L = \mathrm{MSE}(\boldsymbol{s}^{pred}_{task,seq}, \boldsymbol{s}^{ref}_{task,seq}) + \alpha E_{adj}(\boldsymbol{u}^{init}_{seq}) \tag{4}$$

$$\boldsymbol{g} = dL/d\boldsymbol{u}^{init}_{seq} \tag{5}$$

$$\boldsymbol{u}^{init}_{seq} \leftarrow \boldsymbol{u}^{init}_{seq} - \beta \frac{\boldsymbol{g}}{|\boldsymbol{g}|} \tag{6}$$

where $\boldsymbol{u}^{init}_{seq}$ is the sequence of the initial value of control command, $\boldsymbol{s}^{pred}_{task,seq}$ is the predicted sequence of $\boldsymbol{s}_{task}$ in $[t+1, t+N]$ calculated from $\boldsymbol{s}'_{task,t}$ and $\boldsymbol{u}^{init}_{seq}$, and $\boldsymbol{s}^{ref}_{task,seq}$ is a vector arranging $N$ number of $\boldsymbol{s}^{ref}_{task}$. Also, MSE is mean squared error, $E_{adj}$ is MSE of the values at adjacent time steps, $\alpha$ is a weight constant, and $\beta$ is an update rate. We calculate the loss between the predicted and target $\boldsymbol{s}_{task}$, add the loss to smoothen the target control command sequence, and update the control command sequence by backpropagation [19]. By repeating this procedure, $\boldsymbol{u}^{init}_{seq}$ is updated to accurately realize $\boldsymbol{s}^{ref}_{task}$, and the task is executed by sending $\boldsymbol{u}^{init}_{t}$ to the actual robot. While (a) is the network regarding static motions, (b) is the network regarding dynamic motions, and its learning is difficult due to more variables. So, the robot is moved mainly by (a), but (b) is constructed offline and used when conducting tasks in which dynamic and accurate motions are required.

(c) is the reflex module which is executed at high frequency. Muscle Relaxation Control (MRC) [16] is a control elongating muscles from antagonist muscles to agonist muscles while keeping the current joint angle. First, we calculate the necessary muscle tension $\boldsymbol{x}$ achieving the necessary joint torque $\boldsymbol{\tau}^{nec}$ by solving quadratic programming.

$$\underset{\boldsymbol{x}}{\text{minimize}} \quad \boldsymbol{x}^T W_1 \boldsymbol{x} + (G^T \boldsymbol{x} + \boldsymbol{\tau}^{nec})^T W_2 (G^T \boldsymbol{x} + \boldsymbol{\tau}^{nec}) \tag{7}$$

$$\text{subject to} \quad \boldsymbol{x} \geq \boldsymbol{f}^{min} \tag{8}$$

where $W_1, W_2$ are weight matrices, and $\boldsymbol{f}^{min}$ is the minimum muscle tension. We sort muscles by $\boldsymbol{x}$ in ascending order, and gradually elongate them in order starting with unnecessary antagonist muscles with smaller tension. In detail, we gradually increase the muscle relaxation value $\Delta\boldsymbol{l}_{relax}$, and add it to the muscle length to send to the actual robot. When the muscle tension becomes smaller than $\boldsymbol{f}^{min}$, the muscle to elongate is changed to the next muscle, and this control stops when the current joint angle is changed more than a threshold. This procedure works in a static state. At a moving state, we sort muscles by $\boldsymbol{x}$ in descending order, and gradually decrease $\Delta\boldsymbol{l}_{relax}$ starting with necessary muscles. This reflex can inhibit unnecessary muscle tension of antagonist muscles due to the model error. Also, for example, when resting the arms on the table, the body and environment are constrained, and so not only antagonist muscle tension but also agonist muscle tension can be reduced, because the joint angle does not change even when relaxing agonist muscles. Thus, the robot becomes able to rest its body and move continuously for a longer time. Safety reflex is a simple control that elongates muscle length in order not to break motors due to high muscle tension and temperature. We add $\Delta\boldsymbol{l}_{safe}$ calculated as below to the target muscle length,

$$\Delta\boldsymbol{l}^{ref}_{safe} = K_f \max(\boldsymbol{f} - \boldsymbol{f}^{lim}, \boldsymbol{0}) + K_c \max(\boldsymbol{c} - \boldsymbol{c}^{lim}, \boldsymbol{0}) \tag{9}$$

$$\Delta\boldsymbol{l}_{safe} \leftarrow \Delta\boldsymbol{l}_{safe} + \max(\Delta\boldsymbol{l}^{min}, \min(\Delta\boldsymbol{l}^{max}, \Delta\boldsymbol{l}^{ref}_{safe} - \Delta\boldsymbol{l}_{safe})) \tag{10}$$

where $\{\boldsymbol{f}, \boldsymbol{c}\}^{lim}$ is a threshold of muscle tension or temperature to begin the reflex, $K_{\{f,c\}}$ is a gain, $\Delta\boldsymbol{l}^{ref}_{safe}$ is an ideal elongation value, and $\Delta\boldsymbol{l}^{\{min,max\}}$ is a minimum or maximum change of $\Delta\boldsymbol{l}_{safe}$ at one time step. By elongating the muscle length considering muscle tension and temperature, we can inhibit the burnout of motors.

(d) is the recognition module, and it is divided into object and sound recognition. In this study, we use Yolo v3 [20] for object recognition. The labels mainly used in this study is "car," "person," and "traffic light." Also, regarding sound recognition, the sound is converted into a mel spectrum, and the network $\boldsymbol{h}_{sound}$ is trained to output sound class from the spectrum. In this study, this module recognizes only noise or car horn.

### C. Application of the Software to Autonomous Driving

We show the use of each software component for autonomous driving in Fig. 5 (presented in multimedia material).

The static module can be applied to various motions, and especially, is useful for steering wheel operation. In (a), we show an experiment to operate the steering wheel during online learning of the static module. The graphs of (a) show the transition of the steering wheel angle and 10 muscle tensions of the shoulder and elbow of Musashi. At every operation, the angle gradually increases, and muscle tension gradually decreases. Thus, the relationship among $\boldsymbol{f}$, $\boldsymbol{\theta}$, and $\boldsymbol{l}$ is correctly updated using the actual robot sensor information.

The dynamic module is useful for dynamic motions. The pedal operation is a good example because a fast motion adaptation is necessary. In (b), we trained the dynamic module using the data of random pedal operation for one minute and conducted pedal operation with the trained network. This experiment was conducted indoors and the rear wheels were on free rollers for safety. The car velocity was obtained through CAN-USB of the car. We describe the car velocity as $v_{car}$ and the joint angle of right ankle pitch as $\theta_{ankle}$, and set $\theta_{ankle}$ as $\boldsymbol{u}$. We set $v^{ref}_{car} = 5[km/h]$, and conducted the manually tuned PID control (**PID**) and the proposed control with the dynamic module (**Proposed**). When comparing **PID**

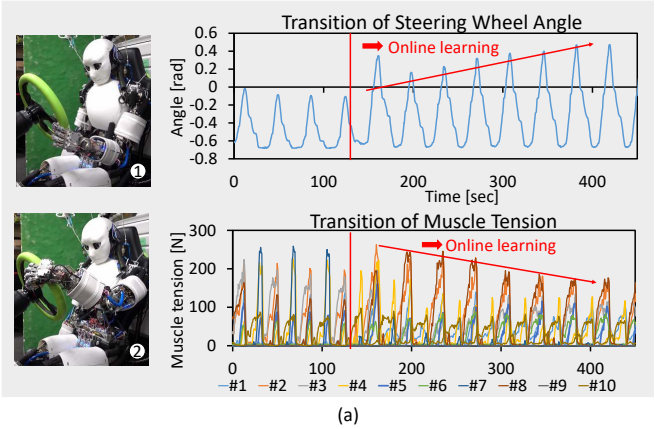


(a)

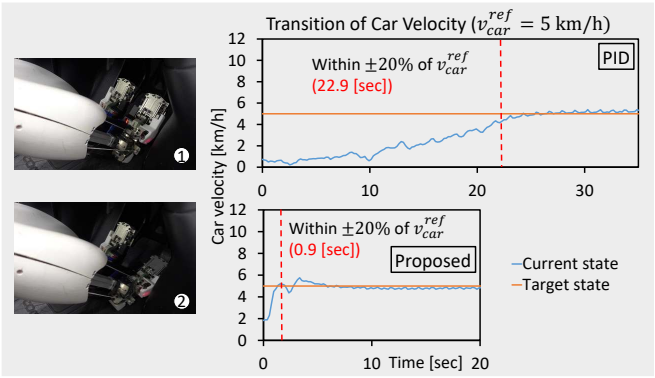


(b)

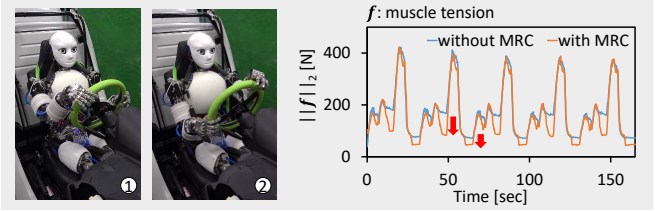


(c)

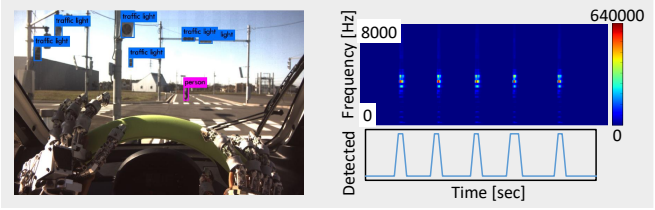


(d)

Fig. 5. Respective components of autonomous driving using the developed software. (a) shows a steering wheel operation experiment using the online learning of static module. (b) shows a pedal operation experiment using the trained dynamic module. (c) shows a steering wheel operation experiment with and without muscle relaxation control. (d) shows visual recognition of traffic lights and a human, and sound recognition of a car horn.

and **Proposed**, the error between $v_{car}$ and $v_{car}^{ref}$ falls within 20% starting from 22.9 sec and 0.9 sec, respectively. Since the dynamic relationship between the joint angle of ankle-pitch and car velocity is complex, this was the limit of **PID** by manual tuning and the car velocity vibrated largely when further increasing the gain in our experiment. Thus, by acquiring the state equation between task state and control

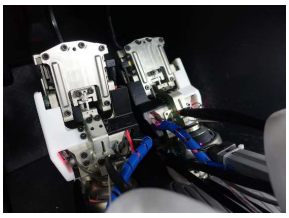

(a)

(b)

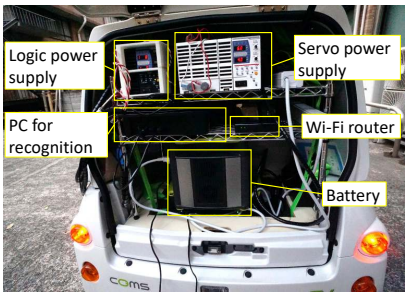


(c)

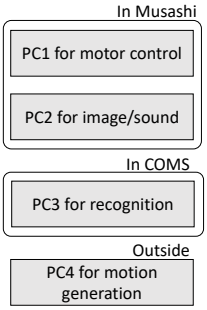


(d)

Fig. 6. Experimental setup of autonomous driving by the musculoskeletal humanoid Musashi: (a) pedal operation configuration, (b) experimental environment, (c) experimental configuration in COMS, and (d) configuration of PCs.

command, fast tracking is enabled.

The reflex module is useful for motions with long rest time. For example, as shown in (c), during the steering wheel operation, the robot does not always operate the wheel. In this case, Muscle Relaxation Control (MRC) gradually makes antagonist muscles elongate and makes internal force decrease. Also, because the steering wheel and the hands are constrained, the current joint angle does not change largely even when elongating agonist muscles. We show the transition of L2 norm of 10 muscle tensions of the elbow and shoulder in the left arm of Musashi $||\boldsymbol{f}||_2$, with and without MRC. The muscle tension is reduced in a static state with MRC compared to without MRC. This module can inhibit the increase of muscle temperature, and long-time operation is enabled.

The recognition module is mainly used as visual recognition of "person" and "traffic light," and sound recognition of the car horn. The left figure of (d) shows the recognition result at a crossing, and the traffic lights and a human are recognized well. Also, the right figure of (d) shows the sound spectrum of a car horn, and the car horn is recognized well.

## IV. Experiments

### A. Experimental Setup

The car used in this study is a B.COM Delivery of extremely small EV COMS (Chotto Odekake Machimade Suisui) series. For safety, its motor torque is limited to 5 Nm, and an emergency stop button is equipped. In the pedal operation, as shown in (a) of Fig. 6, acceleration and brake pedal is operated by the right and left foot, respectively. The experiment is conducted in the Kashiwa Campus at the University of Tokyo, as shown in (b). As shown in (c), COMS is equipped with a battery, logic power supply, servo

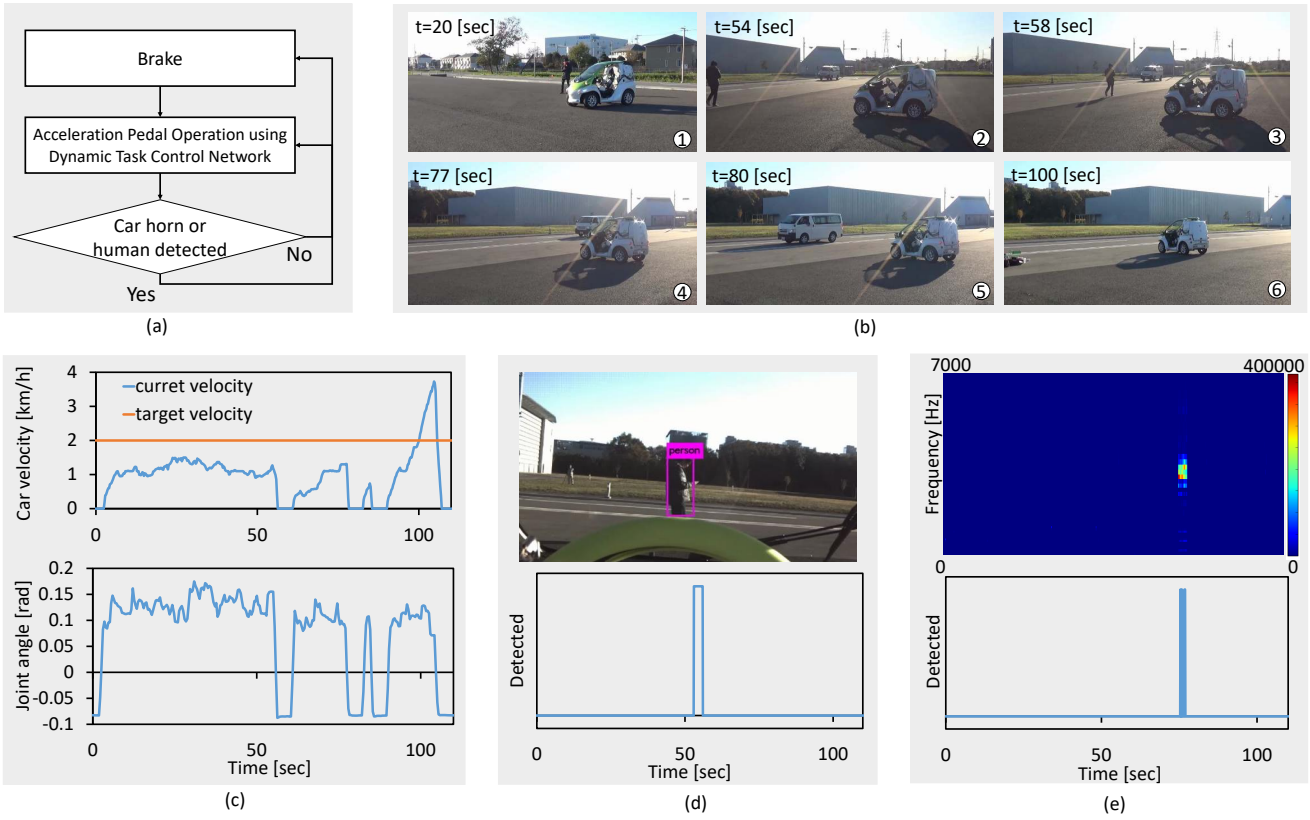


Fig. 7. Pedal operation experiment with recognition. (a) shows the experimental motion flow. (b) shows the experimental appearance. (c) shows the current and target car velocity (upper graph) and the joint angle of the right ankle pitch for the acceleration pedal (lower graph). (d) shows the visual recognition result. (e) shows the sound spectrum and its recognition result.

power supply, Wi-Fi router, and PC for recognition module in the trunk. COMS is an electric vehicle, and all the electric power for the robot can be obtained from COMS in the future. As shown in (d), PCs (Intel NUC, Intel, Inc.) for motor control and image/sound are in the head of Musashi, the recognition is executed on the PC (ZOTAC VR GO, ZOTAC, Inc.) in COMS, and the other processes are executed on PC4 outside.

### *B. Pedal Operation with Recognition*

We conducted an experiment integrating the pedal operation and recognition (Fig. 7, presented in multimedia material). We show the experimental motion flow in (a) of Fig. 7. First, the robot operates the acceleration pedal using the trained dynamic module, steps on the brake pedal if it recognizes a human, restarts the acceleration pedal operation, and steps on the brake pedal again if it recognizes a car horn. The motion sequence is shown in (b) of Fig. 7, and we can see that it succeeded. (c) shows the transition of car velocity (upper graph) and joint angle of the right ankle pitch (lower graph). (d) shows the recognition result of a human. The robot recognizes a human when its bounding box is larger than a certain threshold and its center coordinate is around the center of the image. (e) shows the recognition result of a car horn. When a human (c) or car horn (d) was detected, the brake pedal was stepped on, and we can see that the car velocity became 0. The big problem here is the poor tracking of the target car velocity as shown in (c). This is because of the difference between the environment that the network is trained in and the experimental environment. When $t = [0, 60]$ [sec], the car velocity decreased because the road friction was high, and when $t = [90, 110]$ [sec], the car velocity increased because the road was downhill. This was not a problem in the experiment on the free roller, but the difference of the actual environment was difficult to handle. Because the learning-based controls depend on the data used for training, we must continue to conduct experiments outside, obtain data, and solve this problem.

### *C. Handle Operation with Recognition*

We conducted the steering wheel operation with recognition (Fig. 8, presented in multimedia material). We show the motion flow in (a) of Fig. 8. The robot steps on the brake pedal when the traffic light is red, releases the brake pedal when the traffic light turns blue, and turns right at the crossing by the steering wheel operation with the static module. In this experiment, because turning at a curve is difficult when the car velocity is fast, we use creep velocity just by releasing the brake pedal. Also, the steering wheel is turned to the right first and then is turned to the left by a human command. (b) shows the overview of this experiment, and we can see that the car began to move when the traffic light turned blue and the car could turn right at the crossing by 90 deg. (c) shows the sequence of the steering wheel operation. The sequence is rotating the steering wheel by both arms as much as possible, releasing the left hand,

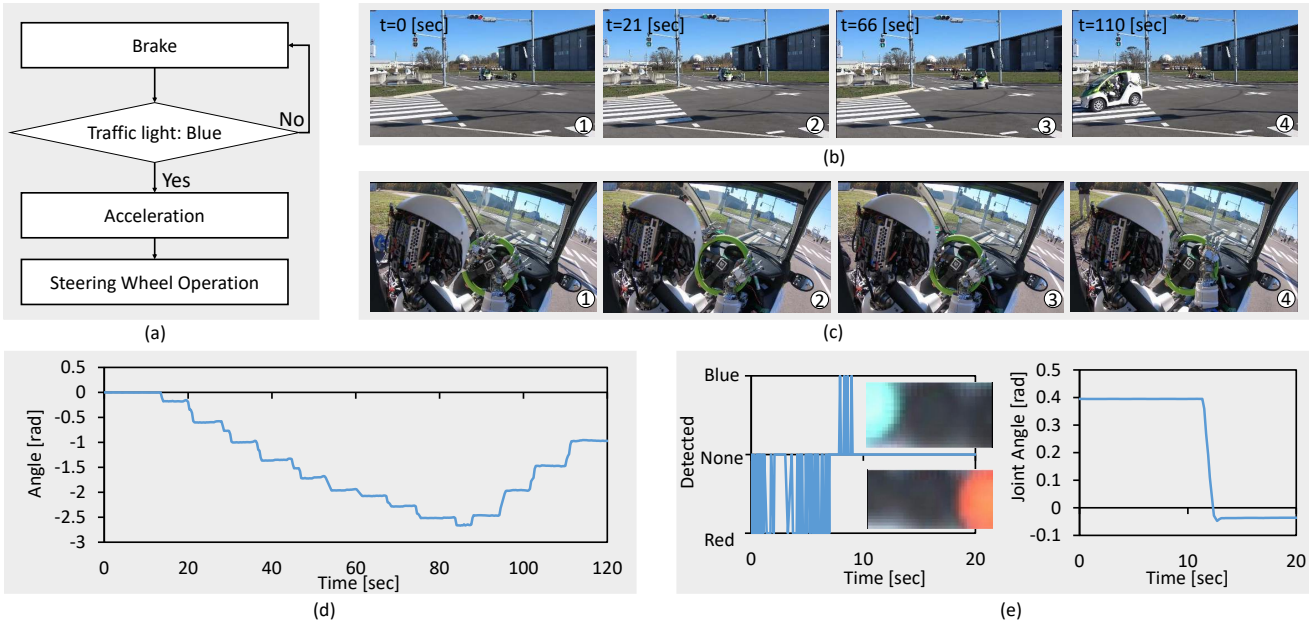


Fig. 8. Steering wheel operation with recognition. (a) shows the experimental motion flow. (b) shows the experimental appearance. (c) shows the sequence of steering wheel operation. (d) shows the transition of the steering wheel angle. (e) shows the traffic light recognition result and the joint angle of the left ankle pitch for brake pedal operation.

returning the left hand to the original position, releasing the right hand, returning the right hand to the original position, and rotating again. The transition of the steering angle is shown in (d). The robot could turn the steering wheel by about 180 deg in 70 sec. The left figure of (e) shows the recognition result of the traffic light. The light is cropped by object detection module, and the blue or red of the traffic light is recognized from the ratio of red and blue pixels. The module could recognize the moment when the light turns from blue to red. At the same time, as shown in the right figure of (e), the left ankle pitch joint moved to release the brake pedal, and the car began to move. The problem of this experiment is the slowness of the steering wheel operation. Currently, turning at the crossing takes about two minutes, and we must make the motions faster and smoother.

## V. Limitations and Future Works

### A. Pedal Operation

The pedal operation is one of the tasks with various remaining issues. In this study, we assumed a flat and smooth road and developed a method to achieve the target car velocity quickly by representing the state equation between the car velocity and joint angle of the ankle pitch. However, there are three issues.

First, in the actual driving environment, the road is not smooth; the ground rises at a crossing, and the road is sometimes uphill or downhill. In those cases, the state equation trained at a flat road is different from that of the actual environment, and the robot cannot adjust the car velocity well. To solve this problem, we need to conduct online learning or add the image of road condition and IMU information in the body to the initial task state $\boldsymbol{s}^{task\prime}$. However, online learning becomes difficult with additional network input, and an efficient learning system with only a few data is desired.

Second, the robot adjusts only the acceleration pedal, and cannot adjust the brake pedal. When driving more slowly than creep velocity, the robot must adjust the car velocity by stepping on the brake pedal. Also, in this study, although not required at the slow car velocity, the robot needs to acquire how to smoothly step on the brake pedal as the car velocity becomes fast.

Third, the car velocity is currently obtained from COMS software, but it should be obtained using image information, IMU, etc. Since the car velocity obtained from visual odometry is too noisy for pedal operation now, especially at low speed, we need to develop a new estimation algorithm.

### B. Steering Wheel Operation

Although Musashi succeeded in the steering wheel operation with both arms for the first time, there remain some issues.

First, in this study, the robot operated the steering wheel not by grasping it but by pressing the hand to it. Releasing and holding the steering wheel were difficult because the fingers sometimes were caught by the wheel or the robot could not accurately grasp the intended part. The first problem is prominent because the complex finger structure is often caught somewhere in the car, and the robot cannot restore itself. The hand structure with smooth skin or a glove may be able to solve this problem. Also, the robot needs to identify the direction its hand was caught from sensors and restore itself.

Second, in this study, the robot operated the steering wheel by push-pull steering method, and it is not the usual human motion of the cross arm steering. In the cross arm steering, the arms move while interfering with each other,

and the inverse kinematics must be solved in a wide range. We experienced that large internal force among the arms sometimes emerges and parts of the hands were caught by each other. Also, we found that the robot must have the scapula joint to solve the inverse kinematics in a wider range.

### C. Recognition

We used the general object detection method for the visual recognition module, and the recognition of the road line and distance to objects are not conducted. Especially, the latter is due to the structure of the developed eye unit. While the movable eye unit can enlarge the field of view by moving the eyes, the external parameter changes by this movement and estimation of the depth map by stereo vision is difficult. Currently, we are developing a learning-based method to estimate the object distance from the convergence angle, binocular parallax, etc. Also, our experiments are conducted only at day time. At night time, although we, humans, can recognize traffic lights and pedestrians through the cameras, Musashi, that is, YOLOv3, cannot. We used the pretrained model of YOLOv3, but the model does not use time-series transition of image and is not trained by using the dataset at the night time. Therefore, we need to train another model using video and dataset at the night time.

Although acoustic information is rarely used for autonomous driving, we applied it to the recognition of the car horn. In the future, we need to develop a system for the robot to understand the current situation by integrating the visual and sound information, to recognize the anomaly of the engine, and to talk with humans.

The recognition of the failure of the hardware components will also become important. In musculoskeletal humanoids, the failure is mainly in the muscle, which can be broken when strong force is applied continuously or when the wire is frayed by friction. By using an Autoencoder-type network, we can detect anomalies, and even if the muscle is ruptured, by continuing online learning, we can obtain the intersensory network in the broken state as in [14]. However, the actual task of autonomous driving requires quicker adaptation and operation in dangerous situations, and the detection of anomalies in hardware components and their handling should be considered more deeply for safety.

### D. Future Works

The content we handled in this study is only a part of the entire system for autonomous driving. The robot must get into the car, localize the self-position with SLAM, and conduct a driving motion planning. Also, the respective components of rotating a key, pulling a handbrake, looking around, acceleration pedal operation, and steering wheel operation must be integrated into one system. For this purpose, we need a method that handles the flexible body more accurately, manages the muscle temperature, and recognizes the situation more accurately. Also, we need to improve the hardware for the scapula with wide range motion and the body shape with smooth human-like skin.

Furthermore, in order to be able to drive not only a single car but also various cars, we have to consider what needs to be learned immediately when a car is changed. It is necessary to learn not only the current intersensory network and dynamic task control network but also the position of key, side brake, etc. in the future.

Finally, this is the first example of a robot sitting on a car and driving a car with both arms without a jig, but some metric is needed to compare its performance in the future. As for performance, we can think of an index of how long it takes to complete a certain course. However, there are many difficult problems such as what kind of course to make and how neatly the course should be driven. As for safety, it is more difficult to establish an index. Although a long-term endurance test is possible, we have not yet reached the stage.

## VI. CONCLUSION

In this study, we focused on autonomous driving by the musculoskeletal humanoid Musashi using the characteristics of its hardware and software. By making use of the flexibility, variable stiffness structure, and several sensors, we succeeded in the steering wheel operation with both arms and human recognition in the side mirror. Also, we proposed a learning-based system handling the flexible body with difficult modeling and succeeded in the pedal and steering wheel operations with recognition. For autonomous driving by humanoids in the future, we would like to develop the next hardware and software using the obtained knowledge.

## REFERENCES


[1] J. Levinson, J. Askeland, J. Becker, J. Dolson, D. Held, S. Kammel, J. Z. Kolter, D. Langer, O. Pink, V. Pratt, M. Sokolsky, G. Stanek, D. Stavens, A. Teichman, M. Werling, and S. Thrun, "Towards fully autonomous driving: Systems and algorithms," in *Proceedings of the 2011 IEEE Intelligent Vehicles Symposium (IV)*, 2011, pp. 163–168.

[2] M. R. Endsley, "Autonomous Driving Systems: A Preliminary Naturalistic Study of the Tesla Model S," *Journal of Cognitive Engineering and Decision Making*, vol. 11, no. 3, pp. 225–238, 2017.

[3] "DARPA Robotics Challenge," http://archive.darpa.mil/roboticschallenge/, Accessed: 2020-03-16.

[4] C. Rasmussen, K. Sohn, Q. Wang, and P. Oh, "Perception and control strategies for driving utility vehicles with a humanoid robot," in *Proceedings of the 2014 IEEE/RSJ International Conference on Intelligent Robots and Systems*, 2014, pp. 973–980.

[5] A. Paolillo, P. Gergondet, A. Cherubini, M. Vendittelli, and A. Kheddar, "Autonomous car driving by a humanoid robot," *Journal of Field Robotics*, vol. 35, no. 2, pp. 169–186, 2018.

[6] H. G. Marques, M. Jäntsh, S. Wittmeier, O. Holland, C. Alessandro, A. Diamond, M. Lungarella, and R. Knight, "ECCE1: the first of a series of anthropomimetic musculoskeletal upper torsos," in *Proceedings of the 2010 IEEE-RAS International Conference on Humanoid Robots*, 2010, pp. 391–396.

[7] Y. Nakanishi, S. Ohta, T. Shirai, Y. Asano, T. Kozuki, Y. Kakehashi, H. Mizoguchi, T. Kurotobi, Y. Motegi, K. Sasabuchi, J. Urata, K. Okada, I. Mizuuchi, and M. Inaba, "Design Approach of Biologically-Inspired Musculoskeletal Humanoids," *International Journal of Advanced Robotic Systems*, vol. 10, no. 4, pp. 216–228, 2013.

[8] Y. Asano, T. Kozuki, S. Ookubo, M. Kawamura, S. Nakashima, T. Katayama, Y. Iori, H. Toshinori, K. Kawaharazuka, S. Makino, Y. Kakiuchi, K. Okada, and M. Inaba, "Human Mimetic Musculoskeletal Humanoid Kengoro toward Real World Physically Interactive Actions," in *Proceedings of the 2016 IEEE-RAS International Conference on Humanoid Robots*, 2016, pp. 876–883.

[9] K. Kawaharazuka, S. Makino, K. Tsuzuki, M. Onitsuka, Y. Nagamatsu, K. Shinjo, T. Makabe, Y. Asano, K. Okada, K. Kawasaki, and M. Inaba, "Component Modularized Design of Musculoskeletal Humanoid Platform Musashi to Investigate Learning Control Systems," in *Proceedings of the 2019 IEEE/RSJ International Conference on Intelligent Robots and Systems*, 2019, pp. 7294–7301.

[10] E. Haug, H. Choi, S. Robin, and M. Beaugonin, "Human Models for Crash and Impact Simulation," in *Computational Models for the Human Body*, ser. Handbook of Numerical Analysis. Elsevier, 2004, vol. 12, pp. 231–452.

[11] T. Makabe, K. Kawaharazuka, K. Tsuzuki, K. Wada, S. Makino, M. Kawamura, A. Fujii, M. Onitsuka, Y. Asano, K. Okada, K. Kawasaki, and M. Inaba, "Development of Movable Binocular High-Resolution Eye-Camera Unit for Humanoid and the Evaluation of Looking Around Fixation Control and Object Recognition," in *Proceedings of the 2018 IEEE-RAS International Conference on Humanoid Robots*, 2018, pp. 840–845.

[12] S. Makino, K. Kawaharazuka, M. Kawamura, A. Fujii, T. Makabe, M. Onitsuka, Y. Asano, K. Okada, K. Kawasaki, and M. Inaba, "Five-Fingered Hand with Wide Range of Thumb Using Combination of Machined Springs and Variable Stiffness Joints," in *Proceedings of the 2018 IEEE/RSJ International Conference on Intelligent Robots and Systems*, 2018, pp. 4562–4567.

[13] K. Shinjo, K. Kawaharazuka, Y. Asano, S. Nakashima, S. Makino, M. Onitsuka, K. Tsuzuki, K. Okada, K. Kawasaki, and M. Inaba, "Foot with a Core-shell Structural Six-axis Force Sensor for Pedal Depressing and Recovering from Foot Slipping during Pedal Pushing Toward Autonomous Driving by Humanoids," in *Proceedings of the 2019 IEEE/RSJ International Conference on Intelligent Robots and Systems*, 2019, pp. 3049–3054.

[14] K. Kawaharazuka, K. Tsuzuki, S. Makino, M. Onitsuka, Y. Asano, K. Okada, K. Kawasaki, and M. Inaba, "Long-time Self-body Image Acquisition and its Application to the Control of Musculoskeletal Structures," *IEEE Robotics and Automation Letters*, vol. 4, no. 3, pp. 2965–2972, 2019.

[15] K. Kawaharazuka, K. Tsuzuki, S. Makino, M. Onitsuka, K. Shinjo, Y. Asano, K. Okada, K. Kawasaki, and M. Inaba, "Task-specific Self-body Controller Acquisition by Musculoskeletal Humanoids: Application to Pedal Control in Autonomous Driving," in *Proceedings of the 2019 IEEE/RSJ International Conference on Intelligent Robots and Systems*, 2019, pp. 813–818.

[16] K. Kawaharazuka, K. Tsuzuki, M. Onitsuka, Y. Koga, Y. Omura, Y. Asano, K. Okada, K. Kawasaki, and M. Inaba, "Reflex-based Motion Strategy of Musculoskeletal Humanoids under Environmental Contact Using Muscle Relaxation Control," in *Proceedings of the 2019 IEEE-RAS International Conference on Humanoid Robots*, 2019, pp. 114–119.

[17] Y. Asano, T. Kozuki, S. Ookubo, K. Kawasaki, T. Shirai, K. Kimura, K. Okada, and M. Inaba, "A Sensor-driver Integrated Muscle Module with High-tension Measurability and Flexibility for Tendon-driven Robots," in *Proceedings of the 2015 IEEE/RSJ International Conference on Intelligent Robots and Systems*, 2015, pp. 5960–5965.

[18] K. Kawaharazuka, S. Makino, M. Kawamura, Y. Asano, Y. Kakiuchi, K. Okada, and M. Inaba, "Human Mimetic Forearm Design with Radioulnar Joint using Miniature Bone-muscle Modules and its Applications," in *Proceedings of the 2017 IEEE/RSJ International Conference on Intelligent Robots and Systems*, 2017, pp. 4956–4962.

[19] D. E. Rumelhart, G. E. Hinton, and R. J. Williams, "Learning representations by back-propagating errors," *nature*, vol. 323, no. 6088, pp. 533–536, 1986.

[20] J. Redmon and A. Farhadi, "YOLOv3: An Incremental Improvement," arXiv:1804.02767, 2018.